NANO LETTERS

pubs.acs.org/NanoLett

Letter

# Excitonic Quantum Coherence in Light Emission from $CsPbBr_3$ Metal-Halide Perovskite Nanocrystals

Dallas Strandell, Carlos Mora Perez, Yifan Wu, Oleg V. Prezhdo, and Patanjali Kambhampati*

Cite This: *Nano Lett.* 2024, 24, 61−66

Read Online

ACCESS | Metrics & More | Article Recommendations | Supporting Information



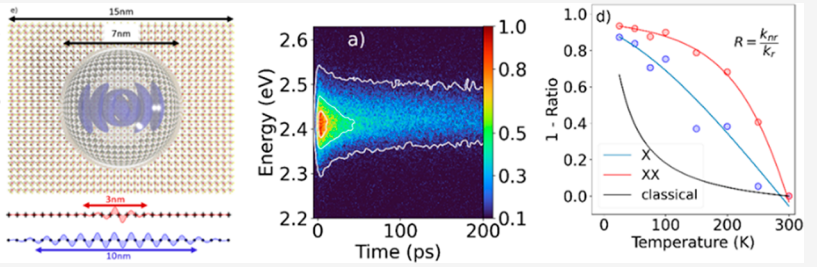


**ABSTRACT:** The decay of excited states via radiative and nonradiative paths is well understood in molecules and bulk semiconductors but less so in nanocrystals. Here, we perform time-resolved photoluminescence (t-PL) experiments on $CsPbBr_3$ metal-halide perovskite nanocrystals, with a time resolution of 3 ps, sufficient to observe the decay of both excitons and biexcitons as a function of temperature. The striking result is that the radiative rate constant of the single exciton increases at low temperatures with an exponential functional form, suggesting quantum coherent effects with dephasing at high temperatures. The opposing directions of the radiative and nonradiative decay rate constants enable enhanced brightening of PL from excitons to biexcitons due to quantum effects, promoting a faster approach to the quantum theoretical limits of light emission. *Ab initio* quantum dynamics simulations reproduce the experimental observations of radiation controlled by quantum spatial coherence enhanced at low temperatures.

**KEYWORDS:** *Quantum dot, nanocrystal, perovskite, exciton, biexciton, photoluminescence, giant oscillator strength*

A ubiquitous process in the study of excited states includes the various pathways for radiative and nonradiative decay. From molecules to bulk semiconductors, these processes have been well studied. In molecules, one has pictures from quantum dynamics described by radiationless transitions, more recently discussed in terms of nonadiabatic dynamics.[1] In bulk semiconductors, one has complementary pictures such as Shockley or Auger processes.[2] In modern quantum materials,[3,4] one aims to understand and implement novel excitonic physics to develop quantum dot lasers,[5] high brightness light emitting diodes,[6] and nonclassical sources of single and entangled photons enabled by quantum coherence in time or space.[7,8]

Nanoscale materials offer the possibility of interpolating between molecular and bulk limits, not just in size but in terms of electronic structure and function toward the applications noted above. Quantum dots (QD), often made of semiconductor nanocrystals (NC), represent a model system for materials in this intermediary regime.[9] Semiconductor perovskite NC (P NC) are less well-studied, a new nanoscale material with remarkable performance in devices from photovoltaics to light-emitting diodes.[10,11] This performance is thought to arise from their remarkable physics of defect tolerance[12,13] arising from liquid/solid duality as a phonon glass/electron crystal.[14−18] In the case of excited state decay, these P NC have been shown to support remarkable light emissive properties such as quantum yields approaching 90% at room temperature.[10,11] Not all metal-halide perovskite (MHP) NC exhibit such high quantum yields, often closer to 50%, with some size dependence that has not yet been solved.[19,20] The MHP NC we explored were synthesized from a variation of the original Kovalenko method and had room temperature quantum yields closer to 50%.[18,21−28] Perhaps the more remarkable observation is of faster decay at low temperature rather than slower, as in most (i.e., classical) cases.[8,29] This initial observation has been rationalized in terms of quantum coherent delocalization giving rise to a giant oscillator strength effect.[29−34] This effect has been discussed in MHP NC and also in CdSe nanoplatelets,[32,34] which have very different physics, thereby suggesting the generality of the effect. There is a lack of observations and insight into the emission of P NC

**Received:** August 23, 2023
**Revised:** December 13, 2023
**Accepted:** December 14, 2023
**Published:** December 19, 2023





https://doi.org/10.1021/acs.nanolett.3c03180
*Nano Lett.* 2024, 24, 61−66

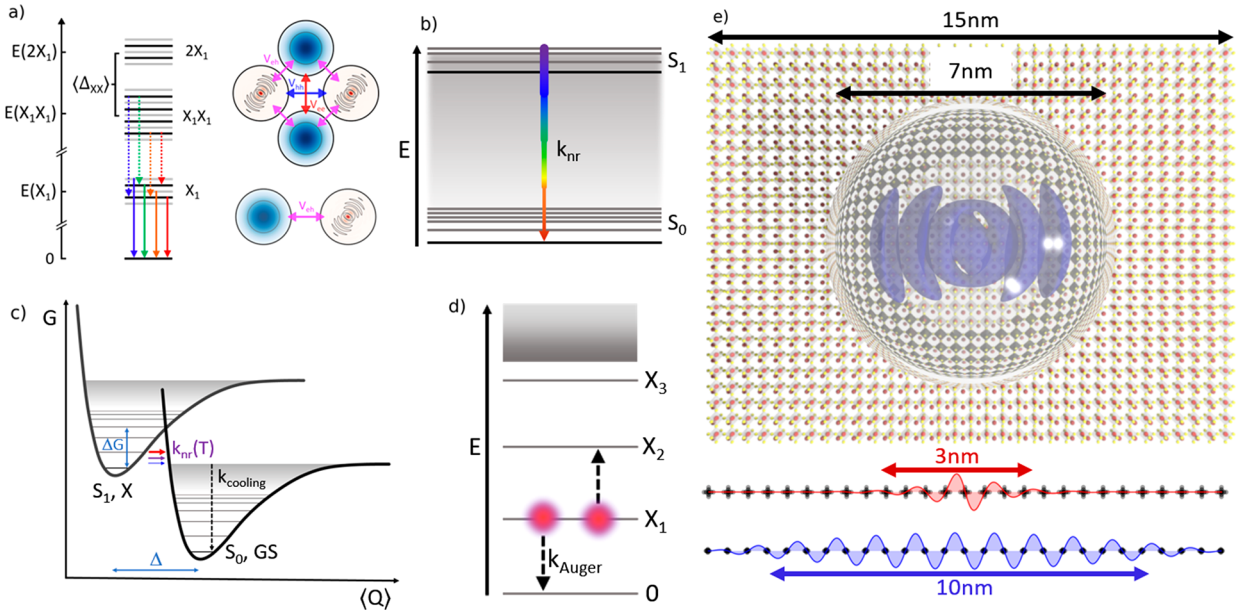


**Figure 1.** Overview of the relationship between excitonic structure, classical nonradiative process, and ideas of quantum delocalization in materials enabling efficient light emission. (a) Overview of exciton (X)/biexciton (XX) structure and charge carrier interactions. The energy of the biexciton is double the single exciton minus the biexciton binding energy ($D_{XX}$), represented by a spectroscopic mean due to their being a manifold of transitions. (b) A simple two-level diagram of excitonic nonradiative recombination misses important information: the temperature dependence of the rate constant. (c) How the temperature dependence of the nonradiative rate constant for X would have an Arrhenius functional form. (d) Schematic illustration of Auger recombination, the path by which XX recombines nonradiatively to X. The temperature dependence of Auger recombination in nanocrystals is not well established. (e) Schematic of an exciton in a nanocrystal showing the length scales involved, from the 15 nm nanocrystal, to the 7 nm Polaron and Bohr lengths, to the idea of thermally induced dephasing of spatial coherence of excitons.

from both excitons and biexcitons. An ability to fully resolve the temperature dependence of the emission kinetics, from excitons to biexcitons, is required in time.

Here, we report on time-resolved photoluminescence (t-PL) spectroscopy of weakly confined (15 nm) $CsPbBr_3$ P NC, at high excitation density to support multiexcitons, with a time resolution of 3 ps, sufficient to resolve the 30 ps kinetics that was previously missed in all prior experiments. In addition to a qualitative leap forward in time resolution, we present data spanning 300−25 000 giving insight into radiative and nonradiative decay mechanisms. We establish these decay mechanisms for excitons (X) and biexcitons (XX). The nonradiative rate constants get slower at lower temperatures, and the radiative rate constants get faster at higher temperatures, for both X and XX. This temperature dependence gives rise to bright PL from X and significantly XX. The radiative decay rate constants have an exponential functional form consistent with thermal fluctuations causing quantum localization. Low temperatures enable quantum coherent spatial delocalization, and the giant oscillator strength effect arises for both X and XX. Notably, the radiative decay constant for XX is identical to that of X at 300 K, but it is twice that of X at 25 K. This observation further suggests low-temperature delocalization, which gives rise to a more strongly correlated XX, having a faster radiative rate constant. This acceleration of radiative rate constants at low temperatures is unique to perovskite NC so far, and it does not arise in model QD NC systems such as CdSe or molecular systems such as laser dyes. Hence, these radiative effects are not trivially due to some excitonic fine structure at low temperatures, whether usual or anomalous, and are proposed to arise from the unique structural dynamics of perovskites. The temperature dependence of the nonradiative rate constants reveals a unimolecular Arrhenius functional form for X, and a bimolecular activated functional form for XX. Ab initio molecular dynamics (AIMD) simulations are performed to rationalize the experiment. The simulations are consistent with the experimental observations on radiative decay and suggest quantum coherent delocalization enabled at low temperatures by freezing out thermal fluctuations.

Figure 1 presents an overview of the salient electronic structure and the resultant kinetic processes. The main idea in QD is that they support confined excitons (X) with a resultant fine structure, as shown in Figure 1a. Unlike molecules and bulk semiconductors, QD also support strongly bound excitonic complexes such as a biexciton (XX).[35,36] The biexciton is lower in energy than twice the exciton energy by a binding energy, $<\Delta_{XX}>$, which must be averaged over the manifold of states as indicated by the bracket.

As discussed in the QD literature, several differences exist between X and XX. One of the main differences is in nonradiative recombination. Nonradiative recombination in molecular or excitonic systems is typically represented as a level diagram with increasing density of vibrational states on the ground electronic state that are isoenergetic with the excited state. Hence, the nonradiative rate constant will be temperature dependent and slow in time, Figure 1b. But in this simple level diagram, the temperature dependence of nonradiative decay is not explicit. Thus, for a more detailed picture, a configuration coordinate diagram is needed which captures the temperature dependence of nonradiative decay, Figure 1c. This diagram allows one to anticipate an Arrhenius functional form for nonradiative decay of X in QD or $S_1$ in molecules.

In the case of XX, one has Auger recombination processes,[2,35,36] which have enhanced rate constants due to


https://doi.org/10.1021/acs.nanolett.3c03180
Nano Lett. 2024, 24, 61−66

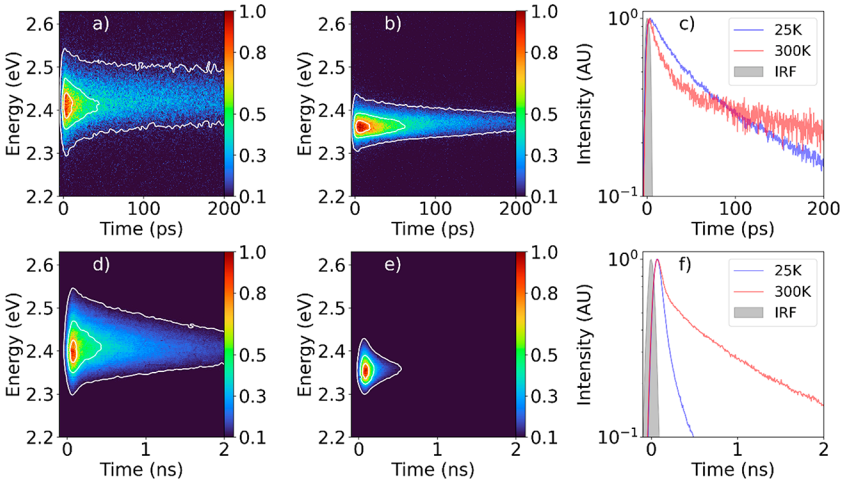


**Figure 2.** Time-resolved photoluminescence (t-PL) of $CsPbBr_3$ nanocrystals with a <$N$> = 3.3 or $f = 1.0 \times 10^{18}$ $cm^{-3}$. Data are shown at two temperatures and two time scales to present an overview. t-PL spectra on the 200 ps time scale at (a) 300 K and (b) 25 K. There are clearly spectral dynamics on the time scale of 30 ps that were previously unresolved. (c) Spectral integration yields kinetic transients with improved signal-to-noise ratio. The transients are biexponential. Cooling the sample from 300 to 25 K causes the fast component to get slower (decay of XX) and the slow component to get faster (decay of X). t-PL spectra on the 2 ns time scale at (d) 300 K and (e) 25 K. (f) Spectrally integrated kinetic transients at both temperatures. The ns time window misses much of the kinetics.

quantum confinement, Figure 1d. In the case of Auger recombination, its size dependence is well-known for the QD, but the temperature dependence remains less well explored. There are two experimental measurements, one using single dot PL[37] and the other using transient absorption spectroscopy.[38] In the case of P NC, the low-temperature acceleration of the radiative rate constant has been rationalized in terms of a longer coherence length enabling a giant oscillator strength.[29] This effect of temperature influencing spatial decoherence of the wave function is illustrated in Figure 1e relative to the 15 nm edge length of these $CsPbBr_3$ P NC. The Bohr length is 7 nm, as is the polaron diameter. The polaron causes lattice distortions about the exciton, as schematically illustrated. The critical question is the length scale of the coherent wave function relative to the localization from the polaron or the physical NC itself.

To explore the effects of temperature on the radiative and nonradiative rate constants for X and XX to unravel possible quantum coherent effects, we perform time-resolved photoluminescence (t-PL) spectroscopy on 15 nm CsPbBr3 NC with a streak camera detector that has an instrument response function of 3 ps, suitable for seeing the fastest PL processes obscured in other experiments with slower detectors. Figure 2 shows the time-resolved photoluminescence (t-PL) of $CsPbBr_3$ nanocrystals with a <$N$> = 3.3 or $f = 1.0 \times 10^{18}$ $cm^{-3}$. The data are shown at two temperatures, 25 and 300 K, and on two time windows, 200 ps and 2 ns. The presence of multiexcitons (MX) is clear from the fast component, a standard signature of MX recombination in QD and NC.[35,39] A spectrally resolved analysis further reveals the details of MX formation and its energetics. See the Supporting Information (SI) for more information about the spectroscopy. Here, we focus on the spectrally integrated kinetic transients. The kinetic transients are shown in Figure 2c and f. The main observation is that the fast component gets slower at low temperatures and the slow component gets faster at low temperatures. See the SI for fit parameters of experimental decay constants as a function of temperature.

The complete temperature dependence of the t-PL kinetics is shown in Figure 3. The radiative and nonradiative rate constants are obtained from the measured decay constants and the quantum yields. See the SI for details. Figure 3a shows the temperature dependence of the nonradiative decay of X, as it is the simplest to understand. The nonradiative rate constants for X have Arrhenius temperature dependence with an activation energy of 3.6 meV and A = 1.9 $ns^{-1}$. Figure 3b shows the nonradiative rate constant for XX, which follows a temperature dependence consistent with bimolecular kinetics. This non-Arrhenius dependence for XX nonradiative rate constants has $E_A$ = 0.54 meV and A = 13 $ns^{-1}$ $K^{-C}$. T with C = 0.28. In both cases, the nonradiative processes follow classical, thermally activated kinetics.

In stark contrast, the radiative rate constants have a temperature dependence in the opposite direction, Figure 3c. The rate constant for X increases at low temperatures with an exponential functional form. The magnitude of the amount is 5.5× from 300 to 25 K. This exponential functional form of temperature dependence is immediately reminiscent of the dephasing of temporal coherences due to temperature, but in this case, one has spatial coherence. The qualitative form of the increase is consistent with the giant oscillator strength effect, in which the excitonic volume increases at low temperatures. This volume increase should result in a specific temperature dependence on the radiative rate constants. The rate constant for XX is precisely the same at 300 K and twice at 25 K. This observation is consistent with more significant spatial coherence and stronger excitonic correlations, giving rise to faster decay of XX. The exact numbers are not the focus of this work and will be discussed elsewhere.

To focus on the quantum advantage enabled by quantum delocalization of excitonic spatial coherence at low temperatures, we plot the PL branching ratio in Figure 3d as $1 - k_{nr}/k_r$. The behaviors of X and XX are shown relative to the classical response. The classical response corresponds to a standard molecular emitter with an Arrhenius temperature dependence for nonradiative decay and no temperature dependence for radiative decay. In the classical case, one


https://doi.org/10.1021/acs.nanolett.3c03180
Nano Lett. 2024, 24, 61−66

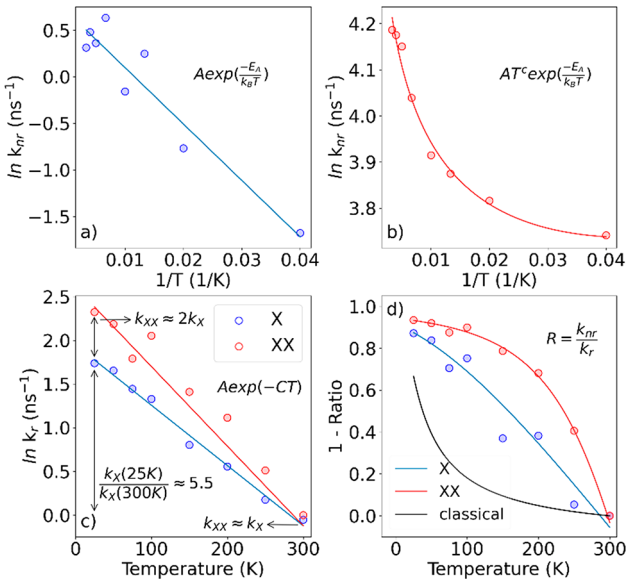


**Figure 3.** Temperature dependence of the rate constants for radiative and nonradiative recombination suggests mechanisms. Conventional classical behavior is seen for nonradiative recombination. In contrast, quantum coherent behavior is seen for radiative recombination. (a) The nonradiative rate constant for X is well fit to a classical Arrhenius model. The nonradiative rate constants for X have Arrhenius temperature dependence with an activation energy of 3.6 meV and A = 1.9 $ns^{-1}$. (b) The nonradiative rate constant for XX follows a temperature dependence consistent with bimolecular kinetics. This non-Arrhenius dependence for XX nonradiative rate constants has $E_A$ = 0.54 meV and A = $^{1}3$ $ns^{-1}$ $K^{-C}$, with C = 0.28. (c) The radiative rate constants follow the opposite temperature dependence and increase at low temperatures, with an exponential functional form that suggests thermal dephasing of quantum coherence. The ratio of these rate constants goes from 1 to 2, over this temperature range. The enhancement of this ratio at low temperatures suggests stronger biexcitonic correlations at low temperatures. (d) The branching ratio shows a temperature dependence for X and XX, in which lower temperatures enable approaching the theoretical limits faster than vial classical light emission.

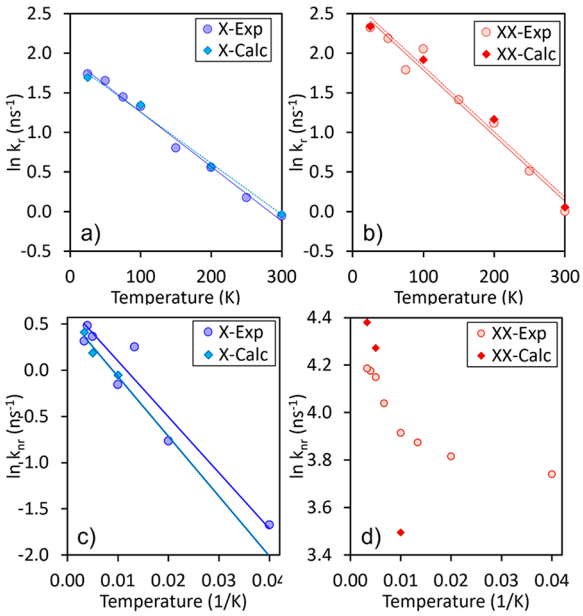


**Figure 4.** AIMD calculations reproduce the experiment. Comparison of the calculated and experimental (a, b) radiative and (c, d) nonradiative decay rates of (a, c) single (X) and (b, d) double (XX) excitons. The calculations match the experimental trends well. The decrease of the radiative rates with increasing temperature arises due to the partial localization of electrons and holes induced by thermal structural disorder, Figure S9. The XX radiative rate shows a stronger dependence on temperature than the X radiative rate because it involves XX coherence that decays faster at higher temperatures, Table S2. The nonradiative X rate exhibits the Arrhenius functional form because it depends on vibrational kinetic energy. The leveling of the nonradiative XX rate at low temperatures is due to nuclear quantum effects, which are more important for XX than X, Figure S10.

interpolates with steep temperature dependence from near zero to near one. In the case of these quantum coherence-enabled emitters, the temperature dependence of X is much shallower, and XX is shallower still. This shallowness to the temperature dependence enables these quantum emitters to get brighter and faster with respect to temperature.

To provide an atomistic interpretation of the experimental results, we perform *ab initio* electronic structure and quantum dynamics calculations, as detailed in the SI. The calculations match the experimental trends, Figure 4, rationalizing the observed temperature dependencies. The radiative decay rates of both X and XX decrease as temperature increases, Figure 4a and b, because of the thermal-induced disorder that partially localizes electrons and holes, Figure S9. The enhanced atomic fluctuations, as shown in Table S1, perturb the symmetry of the crystal lattice, reduce electron−hole overlap, and decrease the transition dipole moments at higher temperatures. The temperature dependence of the radiative rate is stronger for X and XX because the radiative decay of XX is determined by the vector sum of transition dipole moments of the two excitons. The orientations of the transition dipole moments are randomized at higher temperatures, and the XX coherence time decreases, Table S2. This fact suggests that the quantum coherence-enabled emitters (XX) exhibit enhanced brightness and faster decay due to their distinctive temperature-dependent behavior. The finding aligns with previous studies on quantum coherence effects on excitonic dynamics,[40,41] indicating the potential of utilizing quantum coherence for improved optoelectronic applications. The nonradiative decay rates increase with temperature because the process involves coupling to vibrational motions that are enhanced at higher temperatures, Figure 4c and d. The XX nonradiative decay rate flattens at the low temperatures due to nuclear quantum effects, which play a more important role for XX than X. The strongest contribution to the X nonradiative decay arises from a 20 $cm^{-1}$ frequency vibration, corresponding to 30 K, with the influence spectrum decaying rapidly by 100 $cm^{-1}$, Figure S10. In comparison, the electron-vibrational coupling spectrum for XX exhibits signals with similar intensities from 20 to 170 $cm^{-1}$, rationalizing the observed difference in the temperature dependence of the nonradiative decay rates for X and XX, Figure 3.

These experiments and simulations reveal that semiconductor perovskites' unique, defect-tolerant lattice enables their nanocrystals to possess large amplitude quantum coherent effects in their light emission. Spatial delocalization of the excitons at low temperatures enables an accelerated approach toward the theoretical limit for the light emission quantum efficiency. These effects could be useful in sources of


https://doi.org/10.1021/acs.nanolett.3c03180
Nano Lett. 2024, 24, 61−66

single and entangled photons as well as high-brightness light sources.

## ■ ASSOCIATED CONTENT

### Supporting Information

The Supporting Information is available free of charge at https://pubs.acs.org/doi/10.1021/acs.nanolett.3c03180.

Synthetic and experimental details, experimental details for t-PL spectroscopy and modeling (PDF)

## ■ AUTHOR INFORMATION


### Corresponding Author

**Patanjali Kambhampati** − *Department of Chemistry, McGill University, Montreal, Quebec H3A 0B8, Canada;* orcid.org/0000-0003-0146-3544; Phone: +1-514-398-7228; Email: pat.kambhampati@mcgill.ca

### Authors

**Dallas Strandell** − *Department of Chemistry, McGill University, Montreal, Quebec H3A 0B8, Canada*

**Carlos Mora Perez** − *Department of Chemistry, University of Southern California, Los Angeles, California 90089, United States*

**Yifan Wu** − *Department of Chemistry, University of Southern California, Los Angeles, California 90089, United States;* orcid.org/0009-0006-3810-0885

**Oleg V. Prezhdo** − *Department of Chemistry, University of Southern California, Los Angeles, California 90089, United States;* orcid.org/0000-0002-5140-7500

Complete contact information is available at: https://pubs.acs.org/10.1021/acs.nanolett.3c03180


### Author Contributions

Experiments and analysis were done by D. Strandell. Materials were synthesized and characterized by D. Strandell. Calculations were done by C. Mora Perez, Y. Wu, and O. Prezhdo. The manuscript was written by D. Strandell, O. Prezhdo, and P. Kambhampati. P. Kambhampati supervised the work.


### Funding

P. Kambhampati acknowledges financial support from NSERC, CFI, FQRNT, Sony Corporation, and McGill University. O. Prezhdo acknowledges support of the US National Science Foundation, grant CHE-2154367.


### Notes

The authors declare no competing financial interest.

## ■ REFERENCES


(1) Prezhdo, O. V. Modeling non-adiabatic dynamics in nanoscale and condensed matter systems. *Acc. Chem. Res.* **2021**, *54*, 4239−4249.

(2) Melnychuk, C.; Guyot-Sionnest, P. Multicarrier dynamics in quantum dots. *Chem. Rev.* **2021**, *121*, 2325−2372.

(3) Cava, R.; de Leon, N.; Xie, W. Introduction: Quantum Materials. *Chem. Rev.* **2021**, *121*, 2777−2779.

(4) Tokura, Y.; Kawasaki, M.; Nagaosa, N. Emergent functions of quantum materials. *Nat. Phys.* **2017**, *13*, 1056−1068.

(5) Park, Y.-S.; Roh, J.; Diroll, B. T.; Schaller, R. D.; Klimov, V. I. Colloidal quantum dot lasers. *Nature Reviews Materials* **2021**, *6*, 382−401.

(6) Shirasaki, Y.; Supran, G. J.; Bawendi, M. G.; Bulović, V. Emergence of colloidal quantum-dot light-emitting technologies. *Nat. Photonics* **2013**, *7*, 13−23.

(7) Utzat, H.; Sun, W.; Kaplan, A. E.; Krieg, F.; Ginterseder, M.; Spokoyny, B.; Klein, N. D.; Shulenberger, K. E.; Perkinson, C. F.; Kovalenko, M. V.; et al. Coherent single-photon emission from colloidal lead halide perovskite quantum dots. *Science* **2019**, *363*, 1068−1072.

(8) Rainò, G.; Becker, M. A.; Bodnarchuk, M. I.; Mahrt, R. F.; Kovalenko, M. V.; Stöferle, T. Superfluorescence from lead halide perovskite quantum dot superlattices. *Nature* **2018**, *563*, 671−675.

(9) Efros, A. L.; Brus, L. E. Nanocrystal quantum dots: from discovery to modern development. *ACS Nano* **2021**, *15*, 6192−6210.

(10) Akkerman, Q. A.; Rainò, G.; Kovalenko, M. V.; Manna, L. Genesis, Challenges and Opportunities for Colloidal Lead Halide Perovskite Nanocrystals. *Nat. Mater.* **2018**, *17*, 394.

(11) Kovalenko, M. V.; Protesescu, L.; Bodnarchuk, M. I. Properties and Potential Optoelectronic Applications of Lead Halide Perovskite Nanocrystals. *Science* **2017**, *358*, 745.

(12) Dirin, D. N.; Protesescu, L.; Trummer, D.; Kochetygov, I. V.; Yakunin, S.; Krumeich, F.; Stadie, N. P.; Kovalenko, M. V. Harnessing Defect-Tolerance at the Nanoscale: Highly Luminescent Lead Halide Perovskite Nanocrystals in Mesoporous Silica Matrixes. *Nano Lett.* **2016**, *16*, 5866.

(13) Huang, H.; Bodnarchuk, M. I.; Kershaw, S. V.; Kovalenko, M. V.; Rogach, A. L. Lead Halide Perovskite Nanocrystals in the Research Spotlight: Stability and Defect Tolerance. *ACS Energy Lett.* **2017**, *2*, 2071.

(14) Wang, F. F.; Fu, Y. P.; Ziffer, M. E.; Dai, Y. N.; Maehrlein, S. F.; Zhu, X. Y. Solvated Electrons in Solids-Ferroelectric Large Polarons in Lead Halide Perovskites. *J. Am. Chem. Soc.* **2021**, *143*, 5.

(15) Zhu, H. M.; Miyata, K.; Fu, Y. P.; Wang, J.; Joshi, P. P.; Niesner, D.; Williams, K. W.; Jin, S.; Zhu, X. Y. Screening in crystalline liquids protects energetic carriers in hybrid perovskites. *Science* **2016**, *353*, 1409.

(16) Miyata, K.; Atallah, T. L.; Zhu, X. Y. Lead Halide Perovskites: Crystal-Liquid Duality, Phonon Glass Electron Crystals, and Large Polaron Formation. *Sci. Adv.* **2017**, *3*, No. e1701469.

(17) Kambhampati, P. Learning about the Structural Dynamics of Semiconductor Perovskites from Electron Solvation Dynamics. *J. Phys. Chem. C* **2021**, *125*, 23571−23586.

(18) Seiler, H.; Palato, S.; Sonnichsen, C.; Baker, H.; Socie, E.; Strandell, D. P.; Kambhampati, P. Two-dimensional electronic spectroscopy reveals liquid-like lineshape dynamics in CsPbI3 perovskite nanocrystals. *Nat. Commun.* **2019**, *10*, 4962.

(19) Protesescu, L.; Yakunin, S.; Bodnarchuk, M. I.; Krieg, F.; Caputo, R.; Hendon, C. H.; Yang, R. X.; Walsh, A.; Kovalenko, M. V. Nanocrystals of Cesium Lead Halide Perovskites (CsPbX3, X = Cl, Br, and I): Novel Optoelectronic Materials Showing Bright Emission with Wide Color Gamut. *Nano Lett.* **2015**, *15*, 3692.

(20) Akkerman, Q. A.; Nguyen, T. P.; Boehme, S. C.; Montanarella, F.; Dirin, D. N.; Wechsler, P.; Beiglböck, F.; Rainò, G.; Erni, R.; Katan, C.; et al. Controlling the nucleation and growth kinetics of lead halide perovskite quantum dots. *Science* **2022**, *377*, 1406−1412.

(21) Strandell, D. P.; Kambhampati, P. Light Emission from CsPbBr3Metal Halide Perovskite Nanocrystals Arises from Dual Emitting States with Distinct Lattice Couplings. *Nano Lett.* **2023**, *23*, 11330−11336.

(22) Strandell, D. P.; Kambhampati, P. Observing strongly confined multiexcitons in bulk-like CsPbBr3 nanocrystals. *J. Chem. Phys.* **2023**, *158*, 154702 DOI: 10.1063/5.0142113.

(23) Baker, H.; Perez, C. M.; Sonnichsen, C.; Strandell, D.; Prezhdo, O. V.; Kambhampati, P. Breaking Phonon Bottlenecks through Efficient Auger Processes in Perovskite Nanocrystals. *ACS Nano* **2023**, *17*, 3913−3920.

(24) Strandell, D.; Sonnichsen, C.; Kambhampati, P. Watching Excitations in CsPbBr3 Perovskite Nanocrystals Undergo Ultrafast Relaxation to Their Emitting State. *J. Phys. Chem. C* **2022**, *126*, 20505−20510.

(25) Romero Esquivel, G.; Toader, V.; Reven, L.; Kambhampati, P. Ligand-flexible synthesis of strongly confined perovskite nanocrystals: a microwave synthetic approach. *Nanoscale* **2022**, *14*, 15789−15798.

(26) Strandell, D. P.; Kambhampati, P. The Temperature Dependence of the Photoluminescence of CsPbBr3 Nanocrystals Reveals

Phase Transitions and Homogeneous Linewidths. *J. Phys. Chem. C* **2021**, *125*, 27504−27508.
(27) Sonnichsen, C. D.; Strandell, D. P.; Brosseau, P. J.; Kambhampati, P. Polaronic quantum confinement in bulk CsPbBr3 perovskite crystals revealed by state-resolved pump/probe spectroscopy. *Physical Review Research* **2021**, *3*, No. 023147.
(28) Li, B.; Brosseau, P. J.; Strandell, D. P.; Mack, T. G.; Kambhampati, P. Photophysical Action Spectra of Emission from Semiconductor Nanocrystals Reveal Violations to the Vavilov Rule Behavior from Hot Carrier Effects. *J. Phys. Chem. C* **2019**, *123*, 5092.
(29) Becker, M. A.; Vaxenburg, R.; Nedelcu, G.; Sercel, P. C.; Shabaev, A.; Mehl, M. J.; Michopoulos, J. G.; Lambrakos, S. G.; Bernstein, N.; Lyons, J. L.; Stöferle, T.; Mahrt, R. F.; Kovalenko, M. V.; Norris, D. J.; Rainò, G.; Efros, A. L. Bright Triplet Excitons in Caesium Lead Halide Perovskites. *Nature* **2018**, *553*, 189.
(30) Takagahara, T.; Hanamura, E. Giant-oscillator-strength effect on excitonic optical nonlinearities due to localization. *Phys. Rev. Lett.* **1986**, *56*, 2533.
(31) Mahler, B.; Spinicelli, P.; Buil, S.; Quelin, X.; Hermier, J.-P.; Dubertret, B. Towards non-blinking colloidal quantum dots. *Nature materials* **2008**, *7*, 659−664.
(32) Li, Q.; Liu, Q.; Schaller, R. D.; Lian, T. Reducing the optical gain threshold in two-dimensional CdSe nanoplatelets by the giant oscillator strength transition effect. *J. Phys. Chem. Lett.* **2019**, *10*, 1624−1632.
(33) Naeem, A.; Masia, F.; Christodoulou, S.; Moreels, I.; Borri, P.; Langbein, W. Giant exciton oscillator strength and radiatively limited dephasing in two-dimensional platelets. *Phys. Rev. B* **2015**, *91*, No. 121302.
(34) Diroll, B. T.; Schaller, R. D. Reexamination of the Giant Oscillator Strength Effect in CdSe Nanoplatelets. *J. Phys. Chem. C* **2023**, *127*, 4601−4608.
(35) Klimov, V. I. Spectral and Dynamical Properties of Multiexcitons in Semiconductor Nanocrystals. *Annu. Rev. Phys. Chem.* **2007**, *58*, 635.
(36) Kambhampati, P. Multiexcitons in Semiconductor Nanocrystals: A Platform for Optoelectronics at High Carrier Concentration. *J. Phys. Chem. Lett.* **2012**, *3*, 1182.
(37) Benjamin, E.; Yallapragada, V. J.; Amgar, D.; Yang, G.; Tenne, R.; Oron, D. Temperature Dependence of Excitonic and Biexcitonic Decay Rates in Colloidal Nanoplatelets by Time-Gated Photon Correlation. *J. Phys. Chem. Lett.* **2020**, *11*, 6513−6518.
(38) Kobayashi, Y.; Tamai, N. Size-dependent multiexciton spectroscopy and moderate temperature dependence of biexciton auger recombination in colloidal CdTe quantum dots. *J. Phys. Chem. C* **2010**, *114*, 17550−17556.
(39) Makarov, N. S.; Guo, S. J.; Isaienko, O.; Liu, W. Y.; Robel, I.; Klimov, V. I. Spectral and Dynamical Properties of Single Excitons, Biexcitons, and Trions in Cesium-Lead-Halide Perovskite Quantum Dots. *Nano Lett.* **2016**, *16*, 2349.
(40) Mao, L.; Stoumpos, C. C.; Kanatzidis, M. G. Two-Dimensional Hybrid Halide Perovskites: Principles and Promises. *J. Am. Chem. Soc.* **2019**, *141*, 1171−1190.
(41) Srimath Kandada, A. R.; Silva, C. Exciton Polarons in Two-Dimensional Hybrid Metal-Halide Perovskites. *J. Phys. Chem. Lett.* **2020**, *11*, 3173−3184.




https://doi.org/10.1021/acs.nanolett.3c03180
*Nano Lett.* 2024, 24, 61−66